The Tolman Surface Brightness Test for the Reality of the Expansion. III. HST Profile and Surface Brightness Data for Early-Type Galaxies in Three High-Redshift Clusters

Lori M. Lubin[1,2]

Department of Astronomy, California Institute of Technology, Mailstop 105-24, Pasadena, California 91125

Allan Sandage

Observatories of the Carnegie Institution of Washington, 813 Santa Barbara Street, Pasadena, California 91101

ABSTRACT

Photometric data for 34 early-type galaxies in the three high-redshift clusters Cl 1324+3011 ($z = 0.76$), Cl 1604+4304 ($z = 0.90$), and Cl 1604+4321 ($z = 0.92$), observed with the *Hubble Space Telescope* (HST) and with the Keck 10-meter telescopes by Oke, Postman & Lubin, are analyzed to obtain the photometric parameters of mean surface brightness, magnitudes for the growth curves, and angular radii at various Petrosian η radii. The angular radii at $\eta = 1.3$ mag for the program galaxies are all larger than $0\farcs24$. All of the galaxies are well resolved at this angular size using HST whose point-spread function is $0\farcs05$, half width at half maximum. The data for each of the program galaxies are listed at $\eta = 1.0$, 1.3, 1.5, 1.7, and 2.0 mag. They are corrected by color equations and K terms for the effects of redshift to the rest-frame Cape/Cousins I for Cl 1324+3011 and Cl 1604+4304 and R for Cl 1604+4321. The K corrections are calculated from synthetic spectral energy distributions derived from evolving stellar population models of Bruzual & Charlot which have been fitted to the observed broad-band ($BVRI$) AB magnitudes of each program galaxy. The listed photometric data are independent of all cosmological parameters. They are the source data for the Tolman surface brightness test made in Paper IV.

Subject headings: galaxies: clusters: general – cosmology: observations

---

[1]Hubble Fellow

[2]Current address : Department of Physics and Astronomy, Johns Hopkins University, Baltimore, MD 21218

1. Introduction

In the first two papers of this series (Sandage & Lubin 2001, hereafter Paper I; Lubin & Sandage 2001a, hereafter Paper II), we review the Tolman (1930, 1934) surface brightness test for the reality of the expansion. In Paper I, we present the calibration of the diagnostic diagrams at zero redshift of mean surface brightness $\langle SB \rangle$, absolute magnitude M, and linear radius R at various Petrosian (1976) η metric radii. The Petrosian η function is defined as the difference in magnitude between the mean surface brightness averaged over the area interior to a particular radius and the surface brightness at that radius. The unique properties of this function in defining a metric size, which is essential when comparing parameters of galaxies at different redshifts, are described in detail in §2 of Paper I. For the local calibrations, we have used the photometric data of Postman & Lauer (1995) for first ranked cluster galaxies in 118 low redshift Abell clusters. In Paper II, we describe the effect on the profile data of finite angular resolution and the differences in the diagnostic diagrams for early-type galaxies of different flattening ratios.

The purpose of the present paper is to measure the three galaxy parameters of mean surface brightness $\langle SB \rangle$, apparent magnitude m, and angular radius r as a function of the Petrosian radius η for early-type galaxies at high redshift. We have obtained this galaxy sample from the three high-redshift clusters Cl 1324+3011 ($z = 0.76$), Cl 1604+4304 ($z = 0.90$), and Cl 1604+4321 ($z = 0.92$). These clusters were observed with the *Hubble Space Telescope* (HST) by Postman, Lubin, and Oke as discussed by Oke, Postman & Lubin (1998, hereafter OPL), Postman, Lubin & Oke (1998, 2001; hereafter, PLO98 and PLO01), and Lubin et al. (1998, 2001). We have used their extensive photometric data for the present paper. The sample selection and the methods of calculating the $\langle SB(\eta) \rangle$, $m(\eta)$, and $r(\eta)$ functions for these galaxies are given in §2. The method of calculating the photometric K corrections in the Cape/Cousins RI photometric system is given in §3. The surface brightnesses and apparent magnitudes in I for the clusters Cl 1324+3011 and Cl 1604+4304 have been corrected by the $K(I)$ correction to the rest-frame I system. The data in R for Cl 1604+4321 have been corrected by $K(R)$ to the rest-frame R system. These data listed in Tables 5–7 are free from all cosmological assumptions as to world model; however, for the analysis in Lubin & Sandage (2001b, hereafter Paper IV) the absolute magnitude (M) and linear radius (R) values, each which require knowledge of the deceleration parameter q_o, are needed for the comparison of the high-redshift data with the calibrations of the diagnostic diagrams of Paper I. Because the basic observational data in the present paper are cosmological-model free, whereas the analysis in Paper IV is not, we have separated the discussions into the two papers (III here, and IV) to emphasize the difference between the data source presented in this paper with its analysis in Paper IV.

2. Measurements of Mean Surface Brightness, Apparent Magnitude, and Radius for the High-Redshift Early-Type Galaxies

2.1. The Color and Magnitude System

2.1.1. The Keck Observations

The observations by Oke, Postman & Lubin (1998) of the three clusters were made both with the Keck 10-meter telescopes and with HST. The CCD observations at Keck were made in the four photometric passbands that are close to, but not identical with, the standard BV system of Johnson and the RI system of Cape/Cousins (see Figure 1 of OPL). The data on the natural Keck system were reduced to the standard $BVRI$ systems by observing selected standard stars measured by Landolt (1992). These were chosen to be adequately faint in order not to saturate in the short Keck exposures that were taken to determine the color equations.

The importance of the Keck $BVRI$ data for these high-redshift galaxies is that the extended color range permits the choice of an appropriate synthetic spectral energy distribution (SED) of each galaxy from the library of evolved SED models of Bruzual & Charlot (1993). These evolved rest-frame SEDs have been used to calculate the $K(R)$ and $K(I)$ corrections in §3.

2.1.2. The HST Observations

The profile data needed for the calculation of the mean surface brightness $\langle SB \rangle$, apparent magnitude m, and angular radius r at various η values were obtained using HST for the same galaxies observed at the Keck telescopes. Clusters Cl 1324+3011 ($z = 0.76$) and Cl 1604+4304 ($z = 0.90$) were observed using the Wide Field Planetary Camera 2 (WFPC2) in the $F814W$ bandpass, while cluster Cl 1604+4321 ($z = 0.92$) was observed in the $F702W$ bandpass. The color and magnitude equations between these HST filter systems and the standard Cape/Cousins (RI) systems are

$$R = F702W + 0.272(V - R), \tag{1}$$

and

$$I = F814W - 0.05 \text{ for all } (V - I) > 0.7. \tag{2}$$

These equations are the linear approximations to the quadratic equations of Holtzman et al. (1995). They are accurate to better than 0.01 mag.

The sense of equation (1) is that the R magnitudes are fainter than the $F702W$ magnitudes by 0.32 mag at $(V - R) = 1.2$, which is the observed mean $(V - R)$ color of the galaxies in the

three clusters (see Tables 5–7). The sense of equation (2) is that the I magnitudes are brighter by 0.05 mag than the $F814W$ magnitudes of HST in the relevant color range of the galaxies presented here.[3]

2.2. The Sample Selection

To complete the Tolman test, we require a comparison of high-redshift galaxies with the Postman & Lauer (1995) sample of nearby early-type galaxies. Therefore, we have selected our high-redshift sample by choosing only those galaxies which are (1) morphologically classified as early-type galaxies and (2) confirmed members of the three clusters. To satisfy the first criteria, each galaxy had to be morphologically classified from the high-angular-resolution HST images as an early-type, either an elliptical or S0, galaxy by the classifiers in Lubin et al. (1998, 2001).

For the second criteria, the galaxy had either to be a spectroscopically-confirmed cluster member with an elliptical-like (K-star absorption) spectrum, or to have the broad-band colors characteristic of an early-type galaxy at the cluster redshift. The latter criteria essentially uses a photometric redshift technique to identify cluster members (for details, see Brunner & Lubin 2000). In Tables 5–7, we mark those galaxies which are selected based on their photometric, rather than their spectroscopic, redshifts. The resulting samples contain 13, 7, and 14 galaxies in the clusters Cl 1324+3011, Cl 1604+4304, and Cl 1604+4321, respectively.

2.3. The Profile Data and the Three Diagnostic Functions

The two-dimensional HST data were analyzed by the method of ellipse fitting described in §2 of Paper II. Optimized ellipses (i.e. using all the data around the bounding, iterated elliptical contours with optimized pixel width) were fitted to the data by the profile-fitting IRAF task ELLIPSE. These fits produce intensities at a series of increasing radii that could be quantified in several ways. The profile intensities can be listed at (1) the semi-major axis, a, of each ellipse, (2) the "effective" circular radius, $\sqrt{ab}$, where b is the semi-minor axis, or (3) some intermediate radius such as that at 45$^{\rm o}$ from the major axis which has sometimes been used in the literature.

---

[3]It is important to recall (see §2.2 of Sandage 1997) that the Cape/Cousins R system of magnitudes differs substantially from the Johnson R_J system (Johnson 1964, 1965; Johnson et al. 1966), which is the same as the r_{S20} system introduced by Sandage & Smith (1963). $R_J = r_{S20}$ is also the system used by Sandage (1973, Paper V of the redshift-distance series) for the Palomar program on the Hubble diagram for brightest cluster galaxies. The difference between the Cape/Cousins R and R_J is a function of $(V-I)$ given by equations (25) and (26) in Sandage (1997). In the color range of interest for early type galaxies (i.e. $B-V = 1.0$ to 1.1), the Johnson/Sandage magnitudes are 0.25 mag brighter than the Cape/Cousins R magnitudes. This difference must be taken into account when comparing the aperture photometry of Postman & Lauer (1995), which is on the Cape/Cousins R system, with that of Sandage (1973), which is on the R_J system, for cluster galaxies in common to both studies.

In §4 of Paper II we showed that measuring the growth curve using circular apertures was equivalent to using the profile data obtained from the IRAF task ELLIPSE, integrating the data within circular areas of an "effective" radius, $r = \sqrt{ab}$, and listing the data at that $\sqrt{ab}$ radius. Consequently, by using this "equivalent circular" galaxy method, we are able to make an accurate comparison with the local sample of Postman & Lauer (1995) that was originally analyzed using circular apertures. Therefore, for all of the data derived and listed in this paper, we have used the profile data given by the IRAF program ELLIPSE and have integrated this profile with circular apertures of radius, $r = \sqrt{ab}$, rather than the semi-major axis, a.

The total magnitude inside this radius, which defines the growth curve $m(r)$, follows directly from the integrations. Calculation of the Petrosian radius η at various $\sqrt{ab}$ radii follows from the equivalent definition of η of Djorgovski & Spinrad (1981), where η is the difference in magnitudes between the surface brightness averaged over a radius r to the surface brightness (i.e. the profile intensity) at that radius r (see also Sandage & Perelmuter 1990 for a different derivation of this equivalent definition).

We illustrate the calculations using the HST data for three sample galaxies, one from each cluster studied here. Figure 1 shows the HST image of galaxy HST #40 in Cl 1324+3011. This is the ninth-ranked galaxy in the list of 13 galaxies for this cluster (see Table 5). Its total magnitude, derived from the asymptote of the growth curve and using equation (2), is $I = 21.63$. Its half-light radius is $\sqrt{ab} = 0\farcs26$. (Note that the half-light radius for galaxies with normal intensity profiles occurs near $\eta = 1.0$ mag; see Sandage & Perelmuter 1990).

The HST photometric data for this galaxy in the $F814W$ photometric system are listed in Table 1. Column 1 gives the log of the $\sqrt{ab}$ radius. Column 2 lists the $F814W$ surface brightness and the rms error (in magnitudes) of the profile at that radius, as determined by the IRAF program ELLIPSE. Column 3 gives the total magnitude (and error) within a circular aperture of radius $\sqrt{ab}$. This quantity was calculated by integrating the profile data in column 2 within the "effective" circular aperture of radius $\sqrt{ab}$ listed in column 1. These data define the growth curve, $m(r)$. Column 4 lists the mean surface brightness, $\langle SB \rangle$, averaged over the circular aperture with radius $\sqrt{ab}$. It is calculated by adding $5 \times \log(\sqrt{\pi ab})$ to the magnitude in column 3. Column 5 lists the Petrosian η value (and error) calculated by subtracting column 4 from column 2. Column 6 lists the ellipticity, defined as $\epsilon = 1 - \frac{b}{a}$, of the best-fitting ellipse at the listed radius, as determined using the IRAF program ELLIPSE.

Figure 2 shows the four diagnostic curves for HST #40 in Cl 1324+3011, based on the data given in Table 1. The format of these diagrams is the same as Figures 8 and 9 of Paper II. Three of the panels show mean surface brightness $\langle SB \rangle$, apparent magnitude m, and Petrosian radius η versus the "effective" circular radius, $\sqrt{ab}$ (in arcsec). The lower right panel shows $\langle SB \rangle$ versus η.

Figure 3 shows the image of galaxy HST #13 in Cl 1604+4304. This is the third-ranked galaxy of the seven galaxies listed for this cluster in Table 6. Its total magnitude, derived from the asymptote of the growth curve and using equation (2), is $I = 20.68$. Its half-light radius is

0.″36. Table 2 lists the same data as Table 1 but for HST #13 in Cl 1604+4304. Again, the listings are given in the HST $F814W$ photometric system. Figure 4 shows the resulting four diagnostic diagrams.

Figure 5 shows the image of galaxy HST #29 in Cl 1604+4321. This is the second-ranked galaxy of the 14 galaxies listed for this cluster in Table 7. The HST observations were made in the $F702W$ filter. The total magnitude from the asymptote of the growth curve, the observed Keck color of $(V-R)=0.99$ (see Table 7), and equation (1), is $R=22.36$. Its half-light radius is 0.″35. Table 3 lists the same basic data as Tables 1 and 2. Figure 6 shows the four diagnostic diagrams, with the photometry given in the $F702W$ bandpass.

These three galaxies are typical of the program galaxies, although they are neither the brightest nor the faintest in each cluster. The angular radii at $\eta=1$ mag of the 34 program galaxies range from 0.″57 for the largest to 0.″17 for the smallest. It was shown in Paper II that galaxies with half-light radii of 0.″25 should be free from systematic errors larger than $\Delta\langle SB\rangle=0.07$ mag due to the finite point spread function of WFPC2 for all $\eta \gtrsim 1.8$. Hence, the data presented here for $\eta=1.8$ mag and larger should be free of systematic errors due to the finite resolution of HST. For $\eta<1.8$ mag, the data on the smallest galaxies will not be free from some systematic error. We test this prediction in Paper IV where the systematics of the analysis are given for different η values.

All 34 galaxies in the three high-redshift clusters were analyzed in the same ways illustrated in Tables 1–3 and Figures 2, 4, & 6. The data measured at each designated η value for each galaxy in our sample, obtained by a linear interpolation in similar diagrams for each galaxy, are listed in Tables 5–7 (see §4).

3. Calculation of the K Corrections for the Three High-Redshift Clusters

In order to make a comparison with observations of local objects at zero redshift, the K term is a technical correction that must be applied to any observed finite-bandwidth photometry for objects whose spectrum is redshifted (Humason, Mayall & Sandage 1956; Oke & Sandage 1968; Sandage 1995). As defined by these authors, the K term corrects the observed intensity to what would have been observed in the rest frame of the particular photometric band defined by a given filter with its color equation.

The observations by OPL with the Keck telescopes were made with a set of filters whose transmission functions are close to those of the Johnson/Cousins standard $BVRI$ system (see Figure 1 of OPL). The filters, of course, sample the near ultraviolet spectra of the highly redshifted cluster galaxies studied here. For example, the R and I filters with mean wavelengths of 6000Å and 8000Å, respectively, sample the rest-frame spectral energy distributions at the mean rest wavelengths of 3158Å and 4211Å, respectively, for a galaxy at $z=0.90$.

To determine what the observed intensities would have been if the redshifted galaxies had been

observed at the rest-frame wavelengths of the Cape/Cousins RI system, we must know the spectral energy distribution (SED) of the redshifted galaxy in order to tie the observed data at the near-UV and B rest wavelengths to the standard R and I rest wavelengths. Therefore, to calculate the K correction for a given galaxy at redshift of e.g. $z = 0.90$, we need the true SED of that galaxy over the rest wavelength range from 3000Å to the limit of the transmission function of the I filter near 11000Å (Figure 1 of OPL).

The K corrections that have been tabulated in most of the early literature (e.g. Oke & Sandage 1968; Whitford 1971; Yoshii & Takahara 1988; Coleman, Wu & Weedman 1988) used SEDs that were either observed for local, low-redshift galaxies over a large wavelength range or were calculated using stellar population synthesis programs in the no-evolution case. For early-type (elliptical and S0) galaxies, the observed SEDs of elliptical galaxies, such as NGC 4486 or NGC 4472, and/or the central bulge of Sb galaxies, such as M31, were used. These spectra then were redshifted through the filter curves to calculate $K_z(BVRI)$.

However, it became clear from the color indices measured by OPL and analyzed by PLO98 and PLO01 that the observed colors of the high-redshift galaxies used here could not be explained with no-evolution SEDs (see Figure 7). Therefore, to calculate valid K corrections for the galaxies in the three high-redshift clusters, we require knowledge of their actual SEDs, taking into account a luminosity evolution that is a function of wavelength (see Figures 10 & 11 of PLO98).

We have obtained the actual SEDs through work originally performed by Postman, Lubin & Oke to examine the star-formation histories and the ages of the cluster members (PLO98; PLO01). These authors compared the observed broad-band ($BVRI$) AB magnitudes of each galaxy with a measured redshift to synthetic SEDs calculated from the 1996 stellar evolution code of Bruzual & Charlot (1993) under a variety of the star-formation scenarios. Specifically, they used solar metallicity ($Z = 0.02$) models where the star-formation rate falls exponentially with time. These models are referred to as tau (τ) models. A best-fit, zero-redshift SED was calculated for each galaxy using its broad-band AB magnitudes which were blueshifted to the appropriate rest wavelengths by a factor of $(1 + z)$ in $\frac{\Delta\lambda}{\lambda}$ (see PLO98 and PLO01 for details of the fitting procedure).

We note that, over the observed passbands, the final best-fit spectrum is nearly independent of the particular τ model. The largest differences arise at rest UV wavelengths of $\lesssim$ 2500Å which are most sensitive to the youngest stars. This result is illustrated in Figure 7 where we show the best-fit spectrum from a $\tau = 0.2$ Gyr model (solid line) and a $\tau = 0.6$ Gyr model (dotted line) to the observed AB magnitudes of galaxy HST #11 in Cl 1324+3011. The redshift of this galaxy is $z = 0.7580$ (PLO01). The difference in the K correction measured from the two best-fit synthetic SEDs would be only $\Delta K < 0.06$ mag, depending on the particular passband. Consequently, we have adopted for this paper the results from the $\tau = 0.2$ Gyr model of Bruzual & Charlot (1993).

Once an individual SED was adopted for each galaxy, it was used to calculate an individual K correction at the mean redshift of the cluster. This was done by redshifting the adopted rest-wavelength synthetic SED by $(1+z)$ and calculating the intensity ratio of the redshifted SED to the

non-redshifted SED after convolving each with the appropriate filter function from Figure 1 of OPL. Because the effective bandwidth of the shifted SED is smaller than that for the unshifted spectrum by $\frac{\lambda}{1+z}$, the non-selective bandwidth factor of 2.5 $\log(1+z)$ mag must be added to this intensity ratio (expressed in magnitudes). [What we have just described is the explanation of equation (B7) in Appendix B of Humason, Mayall & Sandage (1956), where the theory of the K correction is given in detail.]

We have calculated individual $K(R)$ and $K(I)$ values for each of the early-type galaxies in the three clusters by using the best-fit synthetic Bruzual & Charlot SED based on the individual, observed AB magnitudes. The corrections are not all identical in a given cluster because of variations in the measured magnitudes at different wavelengths which are caused by a combination of measuring errors due to photon statistics and real differences in the intrinsic SEDs. Therefore, we have averaged the individual K corrections for each cluster and have adopted the mean values listed in Table 4. The rms variation in the individual K terms, listed as ΔK in Table 4, are small at $\Delta K \leq 0.08$.

4. K-Corrected Apparent Magnitudes, Mean Surface Brightnesses, and Angular Radii for the Program Galaxies at Five η Values

We have measured the total magnitude m, mean surface brightness $\langle SB \rangle$, and angular radius r at each of the five η values for each galaxy in our sample. These data were derived from the HST profile data in the way described in §2. However, in order to remove some of the stochastic nature of the curves (see e.g. Figures 2, 4 & 6), the measured $SB(r)$, $\langle SB(r) \rangle$, $m(r)$, and $\eta(r)$ functions of each galaxy were smoothed with a three-point boxcar filter. The smoothed curves permitted the growth curve $m(\eta)$, the mean surface brightness $\langle SB(\eta) \rangle$, and the angular radii $r(\eta)$ functions to be interpolated analytically at the discrete values of $\eta = \{1.0, 1.3, 1.5, 1.7, 2.0\}$. These values, corrected by the adopted mean K terms in Table 4, are given in Tables 5–7. We have estimated the error on the total magnitude by adding in quadrature the uncertainties associated with the measured K correction (including both the rms error on the mean value and the uncertainty in the choice of Bruzual & Charlot model; see §3) and our "effective circular" galaxy approximation (see §4.2 of Paper II). These errors also apply to the measurements of mean surface brightness $\langle SB \rangle$.

A reader attentive to details will notice that the entries in Tables 5–7 do not always agree precisely with

$$\langle SB \rangle = m + 5 \log(\sqrt{\pi ab}) \tag{3}$$

which is the definition of mean surface brightness. This equation was used, as described in §2.2, to calculate $\langle SB \rangle$ from the total magnitude, m, and "effective" circular radius, $\sqrt{ab}$, using data tables similar to Tables 1–3. However, the entries in Tables 5–7 are obtained by interpolating the

smoothed curves of the $\langle SB \rangle$, m, and log $\sqrt{ab}$ as a function of η for each of the program galaxies. In the majority of cases, the listed log $\sqrt{ab}$ values in Tables 5–7 are within less than 0.01 dex of the requirement of equation (3). Where there are differences, they are due to the effects of the smoothing of the observed $\langle SB(\eta) \rangle$ and $r(\eta)$ functions which produce small deviations among the measured quantities. Deviations in the log of the linear radius R (used in Paper IV) at the level of 0.007 dex, which is the rms value for the mean deviations from equation (3) of all listed angular radii in Tables 5–7, are totally negligible for the analysis.

The data in Tables 5–7 are the source in the search for a Tolman signal in Paper IV. It is to be emphasized again that the data are independent of any assumptions about cosmological parameters. They are directly observed from the profile data. The η values are metric radii defined by the ratio of surface brightnesses that are measured directly over the face of the galaxy, with no assumption as to any value of a *linear* radius. The apparent magnitudes within the designated η radius requires only a summing of intensities in the pixels interior to that radius.

On the other hand, use of these data for the Tolman test by comparing the $\langle SB \rangle$ values in Tables 5–7 with those of the local galaxies in Paper I requires knowledge of the *absolute* magnitudes, M, and *linear* radii, R. These quantities are needed to produce the diagnostic diagrams of Paper I. The calculations of M and R do require knowledge of the deceleration parameter, q_o, that appears in the Mattig (1958) equations. Although the analysis for the Tolman test is slightly degenerate because of this requirement, we have shown in §5 of Paper I that the resulting hermeneutical circularity is sufficiently small. We shall show this again in Paper IV by comparing the Tolman signals for different assumed q_o values.

We are grateful to Bev Oke and Marc Postman for their kindness in permitting our use of the Oke, Postman & Lubin photometric data for the various calculations before the publication of the complete data in the literature. LML was supported by NASA through Hubble Fellowship grant HF-01095.01-97A from the Space Telescope Science Institute, which is operated by the Association of Universities for Research in Astronomy, Inc., under NASA contract NAS 5-26555. AS acknowledges support for publication from NASA grants GO-5427.01-93A and GO-06459.01-95A for work that is related to data taken with the *Hubble Space Telescope*.

REFERENCES

Brunner, R. & Lubin, L.M.. 2000, AJ, 120, 2851

Bruzual, A.G. & Charlot, S. 1993, ApJ, 405, 538

Coleman, G.D., Wu. C.-C., & Weedman, D.W. 1988, ApJS, 43, 393

Djorgovski, G., & Spinrad, H. 1981, ApJ, 251, 417

Holtzman, J. et al. 1995, PASP, 107, 1065

Humason, M.L., Mayall, N.U., & Sandage, A. 1956, AJ, 61, 97

Johnson, H.L. 1964, Bol. Obs. Ton. Tac., 3, 305

Johnson, H.L. 1965, ApJ, 141, 170

Johnson, H.L., Mitchell, R.T., Iriarte, B., & Wisniewski, W.A. 1966, Comm. Lunar Planet. Lab, No. 63

Landolt, A.U. 1992, AJ, 104, 340

Lubin, L.M. & Sandage, A. 2001a, AJ, 121, 2289 (Paper II)

Lubin, L.M. & Sandage, A. 2001b, AJ, in press (Paper IV)

Lubin, L.M., Postman, M., Oke, J.B., Ratnatunga, K.U., Gunn, J.E., Hoessel, J.G., & Schneider, D.P. 1998, AJ, 116, 584

Lubin, L.M., Postman, M., Oke, J.B., Brunner, R., Gunn, J.E., & Schneider, D.P. 2001, AJ, in preparation

Mattig, W. 1958, Astron. Nach., 284, 109

Oke, J.B., Postman, M., & Lubin, L.M. 1998, AJ, 116, 549 (OPL)

Oke, J.B. & Sandage, A. 1968, ApJ, 154, 21

Petrosian, V. 1976, ApJ, 209, L1

Postman, M. & Lauer, T. 1995, ApJ, 440, 28

Postman, M., Lubin, L.M., & Oke, J.B. 1998, AJ, 116, 560 (PLO98)

Postman, M., Lubin, L.M., & Oke, J.B. 2001, AJ, in press (PLO01)

Sandage, A. 1973, ApJ, 183, 711

Sandage, A. 1995, in The Deep Universe, "Practical Cosmology: Inventing the Past," 23rd Sass Fee Advanced Course in Astrophysics, ed. B. Binggeli & R. Buser, (Springer: Berlin)

Sandage, A. 1997, PASP, 109, 1193

Sandage, A. & Lubin, L.M. 2001, AJ, 121, 2271 (Paper I)

Sandage, A. & Perelmuter, J.-M. 1990, ApJ, 350, 481

Sandage, A. & Smith, L.L. 1963, ApJ, 137, 1057

Tolman, R.C. 1930, Proc. Nat. Acad. Sci, 16, 511

Tolman, R.C. 1934, Relativity, Thermodynamics, & Cosmology, (Oxford: Oxford University Press), p 467

Whitford, A.E. 1971, ApJ, 169, 215

Yoshii, Y. & Takahara, F. 1988, ApJ, 326, 1

AAS LaTeX macros v5.0.

Table 1. Derived Photometric Parameters for HST #40 in Cl 1324+3011 (HST $F814W$ Band)

Log $\sqrt{ab}$ (arcsec) (1)	$SB \pm \Delta SB$ (mag/arcsec^2) (2)	$m \pm \Delta m$ (mag) (3)	$\langle SB \rangle$ (mag/arcsec^2) (4)	$\eta \pm \Delta\eta$ (mag) (5)	ϵ (6)
−1.003	20.05 ± 0.01	23.070 ± 0.014	19.297	0.75 ± 0.02	0.006
−0.710	21.15 ± 0.01	22.503 ± 0.010	20.196	0.96 ± 0.02	0.041
−0.560	21.89 ± 0.01	22.266 ± 0.008	20.706	1.18 ± 0.01	0.152
−0.448	22.42 ± 0.01	22.108 ± 0.007	21.109	1.32 ± 0.01	0.201
−0.355	22.93 ± 0.01	21.993 ± 0.007	21.462	1.47 ± 0.01	0.213
−0.284	23.29 ± 0.02	21.913 ± 0.006	21.735	1.56 ± 0.02	0.243
−0.222	23.63 ± 0.02	21.847 ± 0.006	21.981	1.65 ± 0.02	0.259
−0.163	24.00 ± 0.02	21.793 ± 0.006	22.219	1.78 ± 0.03	0.258
−0.106	24.47 ± 0.04	21.750 ± 0.006	22.464	2.01 ± 0.04	0.235
−0.058	24.80 ± 0.05	21.718 ± 0.006	22.670	2.13 ± 0.05	0.229
−0.017	25.17 ± 0.07	21.694 ± 0.006	22.853	2.32 ± 0.07	0.229
0.018	25.46 ± 0.08	21.677 ± 0.006	23.008	2.45 ± 0.08	0.240
0.031	25.56 ± 0.08	21.670 ± 0.006	23.068	2.49 ± 0.08	0.312
0.063	25.80 ± 0.10	21.656 ± 0.006	23.215	2.59 ± 0.10	0.312
0.101	26.05 ± 0.10	21.640 ± 0.006	23.389	2.66 ± 0.10	0.286
0.129	26.30 ± 0.14	21.629 ± 0.006	23.519	2.78 ± 0.14	0.286
0.156	26.83 ± 0.16	21.623 ± 0.006	23.643	3.19 ± 0.16	0.286
0.180	26.80 ± 0.20	21.615 ± 0.006	23.760	3.04 ± 0.20	0.286
0.204	27.34 ± 0.36	21.611 ± 0.006	23.873	3.46 ± 0.36	0.286

Table 2. Derived Photometric Parameters for HST #13 in Cl 1604+4304 (HST $F814W$ Band)

Log $\sqrt{ab}$ (arcsec) (1)	$SB \pm \Delta SB$ (mag/arcsec^2) (2)	$m \pm \Delta m$ (mag) (3)	$\langle SB \rangle$ (mag/arcsec^2) (4)	$\eta \pm \Delta\eta$ (mag) (5)	ϵ (6)
−1.029	20.07 ± 0.01	23.223 ± 0.006	19.319	0.75 ± 0.01	0.119
−0.734	20.59 ± 0.01	22.369 ± 0.006	19.942	0.65 ± 0.01	0.142
−0.552	21.18 ± 0.01	21.923 ± 0.005	20.407	0.77 ± 0.01	0.117
−0.425	21.73 ± 0.01	21.666 ± 0.004	20.783	0.95 ± 0.01	0.111
−0.326	22.24 ± 0.01	21.498 ± 0.004	21.109	1.13 ± 0.01	0.103
−0.246	22.71 ± 0.01	21.384 ± 0.003	21.395	1.32 ± 0.01	0.100
−0.180	23.15 ± 0.01	21.305 ± 0.003	21.645	1.50 ± 0.01	0.104
−0.122	23.54 ± 0.01	21.244 ± 0.003	21.875	1.66 ± 0.01	0.103
−0.077	23.81 ± 0.01	21.201 ± 0.003	22.056	1.76 ± 0.01	0.129
−0.031	24.17 ± 0.02	21.162 ± 0.003	22.252	1.92 ± 0.02	0.125
0.004	24.41 ± 0.02	21.136 ± 0.003	22.398	2.01 ± 0.02	0.153
0.038	24.65 ± 0.02	21.112 ± 0.003	22.546	2.11 ± 0.02	0.165
0.075	24.90 ± 0.02	21.088 ± 0.003	22.707	2.19 ± 0.02	0.156
0.102	25.12 ± 0.03	21.073 ± 0.003	22.824	2.30 ± 0.03	0.178
0.132	25.44 ± 0.04	21.058 ± 0.003	22.959	2.48 ± 0.04	0.178
0.185	25.80 ± 0.06	21.035 ± 0.003	23.201	2.60 ± 0.06	0.079
0.207	25.92 ± 0.07	21.025 ± 0.003	23.303	2.61 ± 0.07	0.095
0.218	25.89 ± 0.06	21.020 ± 0.003	23.353	2.54 ± 0.06	0.150

Table 3. Derived Photometric Parameters for HST #29 in Cl 1604+4321 (HST $F702W$ Band)

Log $\sqrt{ab}$ (arcsec) (1)	$SB \pm \Delta SB$ (mag/arcsec^2) (2)	$m \pm \Delta m$ (mag) (3)	$\langle SB \rangle$ (mag/arcsec^2) (4)	$\eta \pm \Delta\eta$ (mag) (5)	ϵ (6)
−1.051	21.27 ± 0.01	24.536 ± 0.006	20.522	0.75 ± 0.01	0.204
−0.715	21.64 ± 0.01	23.418 ± 0.004	21.083	0.56 ± 0.01	0.066
−0.539	22.08 ± 0.01	22.907 ± 0.004	21.453	0.62 ± 0.01	0.066
−0.414	22.64 ± 0.01	22.623 ± 0.003	21.795	0.84 ± 0.01	0.064
−0.319	23.21 ± 0.01	22.456 ± 0.003	22.106	1.11 ± 0.01	0.070
−0.240	23.74 ± 0.01	22.347 ± 0.003	22.392	1.35 ± 0.02	0.071
−0.176	24.19 ± 0.03	22.274 ± 0.004	22.637	1.56 ± 0.03	0.085
−0.120	24.53 ± 0.03	22.216 ± 0.004	22.859	1.67 ± 0.03	0.094
−0.072	24.94 ± 0.04	22.175 ± 0.004	23.057	1.88 ± 0.04	0.108
−0.046	25.04 ± 0.06	22.152 ± 0.004	23.166	1.88 ± 0.06	0.183
0.008	25.26 ± 0.06	22.106 ± 0.004	23.388	1.88 ± 0.06	0.137
0.046	25.64 ± 0.07	22.080 ± 0.005	23.550	2.09 ± 0.07	0.137
0.067	25.80 ± 0.08	22.065 ± 0.005	23.644	2.16 ± 0.08	0.187
0.099	26.08 ± 0.11	22.046 ± 0.005	23.786	2.29 ± 0.11	0.187
0.129	26.00 ± 0.09	22.025 ± 0.005	23.915	2.09 ± 0.09	0.187

Table 4. Adopted K-Corrections in Cape/Cousins R and I Bands for the Three Clusters

Cluster	z	$K(R) \pm \Delta K(R)$ (mag)	$K(I) \pm \Delta K(I)$ (mag)
1324+3011	0.7565	1.59 ± 0.04	0.71 ± 0.03
1604+4304	0.8967	1.70 ± 0.08	0.80 ± 0.07
1604+4321	0.9243	1.89 ± 0.06	1.00 ± 0.05

Table 5. Observed Data for Cl 1324+3011 [I Band; $K(I) = 0.71$]

Gal	$\eta = 1.0$			$\eta = 1.3$			$\eta = 1.5$			
#	$I^{\rm b}$	$\langle SB \rangle^{\rm b}$	Log r''	$I^{\rm b}$	$\langle SB \rangle^{\rm b}$	Log r''	$I^{\rm b}$	$\langle SB \rangle^{\rm b}$	Log r''	I
9	20.34 ± 0.07	19.11	-0.485	19.54 ± 0.05	20.75	-0.005	19.11 ± 0.04	21.87	$+0.384$	$\cdots$
11	20.36 ± 0.07	19.89	-0.336	19.70 ± 0.05	21.21	$+0.054$	19.46 ± 0.04	21.82	$+0.226$	19.39 ±
12	20.26 ± 0.06	20.27	-0.243	20.03 ± 0.05	20.73	-0.108	19.94 ± 0.05	20.97	-0.044	19.89 ±
18	20.88 ± 0.07	19.65	-0.486	20.52 ± 0.05	20.39	-0.272	20.37 ± 0.05	20.81	-0.161	20.25 ±
21	21.12 ± 0.08	19.36	-0.583	20.66 ± 0.06	20.31	-0.307	20.49 ± 0.05	20.81	-0.176	20.37 ±
26	21.33 ± 0.07	20.20	-0.464	20.69 ± 0.05	21.44	-0.094	20.55 ± 0.05	21.82	$+0.002$	20.45 ±
29	21.10 ± 0.06	20.36	-0.391	20.74 ± 0.05	21.08	-0.168	20.57 ± 0.04	21.55	-0.059	20.32 ±
30[c]	21.15 ± 0.07	20.52	-0.364	20.96 ± 0.05	20.93	-0.253	20.85 ± 0.05	21.22	-0.170	20.75 ±
40	21.79 ± 0.07	19.42	-0.681	21.38 ± 0.05	20.28	-0.463	21.20 ± 0.05	20.81	-0.322	21.08 ±
55[c]	22.14 ± 0.07	20.50	-0.562	21.88 ± 0.05	21.04	-0.408	21.79 ± 0.05	21.31	-0.339	21.74 ±
59	21.97 ± 0.08	19.73	-0.665	21.68 ± 0.05	20.30	-0.515	21.58 ± 0.04	20.57	-0.445	21.53 ±
69	22.09 ± 0.04	19.24	-0.801	21.86 ± 0.06	19.76	-0.654	21.77 ± 0.04	20.05	-0.583	21.71 ±
74[c]	22.30 ± 0.07	21.28	-0.440	22.00 ± 0.05	21.91	-0.262	21.85 ± 0.05	22.34	-0.146	21.65 ±

[a]Keck colors computed from the total magnitudes measured in matched apertures for each individual band (se

[b]Values have been corrected with the appropriate K correction (see Table 4).

[c]Member galaxy selected based on its photometric redshift (see Brunner & Lubin 2000).

Table 6. Observed Data for Cl 1604+4304 [I Band; $K(I) = 0.80$]

Gal	$\eta = 1.0$			$\eta = 1.3$			$\eta = 1.5$			
#	$I^{\rm b}$	$\langle SB \rangle^{\rm b}$	Log r''	$I^{\rm b}$	$\langle SB \rangle^{\rm b}$	Log r''	$I^{\rm b}$	$\langle SB \rangle^{\rm b}$	Log r''	I
9	20.73 ± 0.10	20.59	-0.273	20.25 ± 0.10	21.55	$+0.014$	20.08 ± 0.09	22.03	$+0.138$	19.99 ±
10[c]	20.85 ± 0.10	20.90	-0.237	20.38 ± 0.10	21.82	$+0.039$	20.26 ± 0.09	22.16	$+0.134$	20.17 ±
13	20.80 ± 0.10	20.00	-0.399	20.56 ± 0.10	20.50	-0.255	20.46 ± 0.09	20.80	-0.178	20.38 ±
34[c]	21.91 ± 0.10	20.98	-0.429	21.62 ± 0.09	21.60	-0.250	21.47 ± 0.09	22.03	-0.139	21.39 ±
46[c]	21.96 ± 0.11	20.40	-0.546	21.72 ± 0.10	20.90	-0.411	21.63 ± 0.09	21.17	-0.335	21.55 ±
50	22.14 ± 0.11	21.11	-0.445	21.79 ± 0.10	21.83	-0.235	21.58 ± 0.09	22.43	-0.069	21.50 ±
58[c]	22.25 ± 0.10	20.65	-0.553	22.03 ± 0.09	21.11	-0.425	21.94 ± 0.09	21.37	-0.355	21.87 ±

[a]Keck colors computed from the total magnitudes measured in matched apertures for each individual band (se

[b]Values have been corrected with the appropriate K correction (see Table 4).

[c]Member galaxy selected based on its photometric redshift (see Brunner & Lubin 2000).

Table 7. Observed Data for Cl 1604+4321 [R Band; $K(R) = 1.89$]

Gal	$\eta = 1.0$			$\eta = 1.3$			$\eta = 1.5$			
#	$R^{\rm b}$	$\langle SB\rangle^{\rm b}$	Log r''	$R^{\rm b}$	$\langle SB\rangle^{\rm b}$	Log r''	$R^{\rm b}$	$\langle SB\rangle^{\rm b}$	Log r''	R
23[c]	20.91 ± 0.10	18.48	-0.702	20.58 ± 0.09	19.16	-0.517	20.47 ± 0.09	19.49	-0.433	20.39 ±
29[c]	20.93 ± 0.10	20.35	-0.358	20.76 ± 0.09	20.71	-0.252	20.67 ± 0.09	20.97	-0.184	20.60 ±
36	21.58 ± 0.10	20.24	-0.506	21.22 ± 0.09	20.97	-0.294	21.10 ± 0.08	21.34	-0.199	20.99 ±
38	21.41 ± 0.10	20.21	-0.475	21.17 ± 0.09	20.71	-0.343	21.07 ± 0.08	21.02	-0.260	20.98 ±
44[c]	21.57 ± 0.09	21.06	-0.340	21.20 ± 0.09	21.76	-0.136	21.09 ± 0.09	22.10	-0.045	21.00 ±
46	21.74 ± 0.10	21.20	-0.345	21.41 ± 0.09	21.89	-0.148	21.27 ± 0.08	22.27	-0.047	21.18 ±
49	22.09 ± 0.10	20.07	-0.623	21.48 ± 0.09	21.33	-0.279	21.33 ± 0.09	21.77	-0.156	21.24 ±
57	21.89 ± 0.10	21.65	-0.290	21.46 ± 0.09	22.50	-0.039	21.25 ± 0.09	23.05	$+0.103$	21.16 ±
58	22.16 ± 0.10	20.38	-0.581	21.80 ± 0.09	21.11	-0.379	21.59 ± 0.09	21.72	-0.219	21.37 ±
65	21.94 ± 0.10	19.83	-0.648	21.64 ± 0.09	20.44	-0.485	21.54 ± 0.08	20.74	-0.411	21.47 ±
78[c]	22.51 ± 0.10	20.70	-0.590	22.18 ± 0.09	21.40	-0.397	22.04 ± 0.09	21.80	-0.283	21.90 ±
112[c]	22.75 ± 0.10	20.27	-0.707	22.44 ± 0.09	20.94	-0.543	22.34 ± 0.08	21.27	-0.449	22.25 ±
115[c]	22.88 ± 0.09	21.09	-0.601	22.49 ± 0.10	21.87	-0.370	22.40 ± 0.08	22.14	-0.308	22.33 ±
144[c]	23.03 ± 0.10	20.74	-0.680	22.67 ± 0.09	21.49	-0.465	22.56 ± 0.09	21.82	-0.390	22.46 ±

[a]Observed Keck colors computed from the total magnitudes measured in matched apertures for each individua

[b]Values have been corrected with the appropriate K correction (see Table 4).

[c]Member galaxy selected based on its photometric redshift (see Brunner & Lubin 2000).

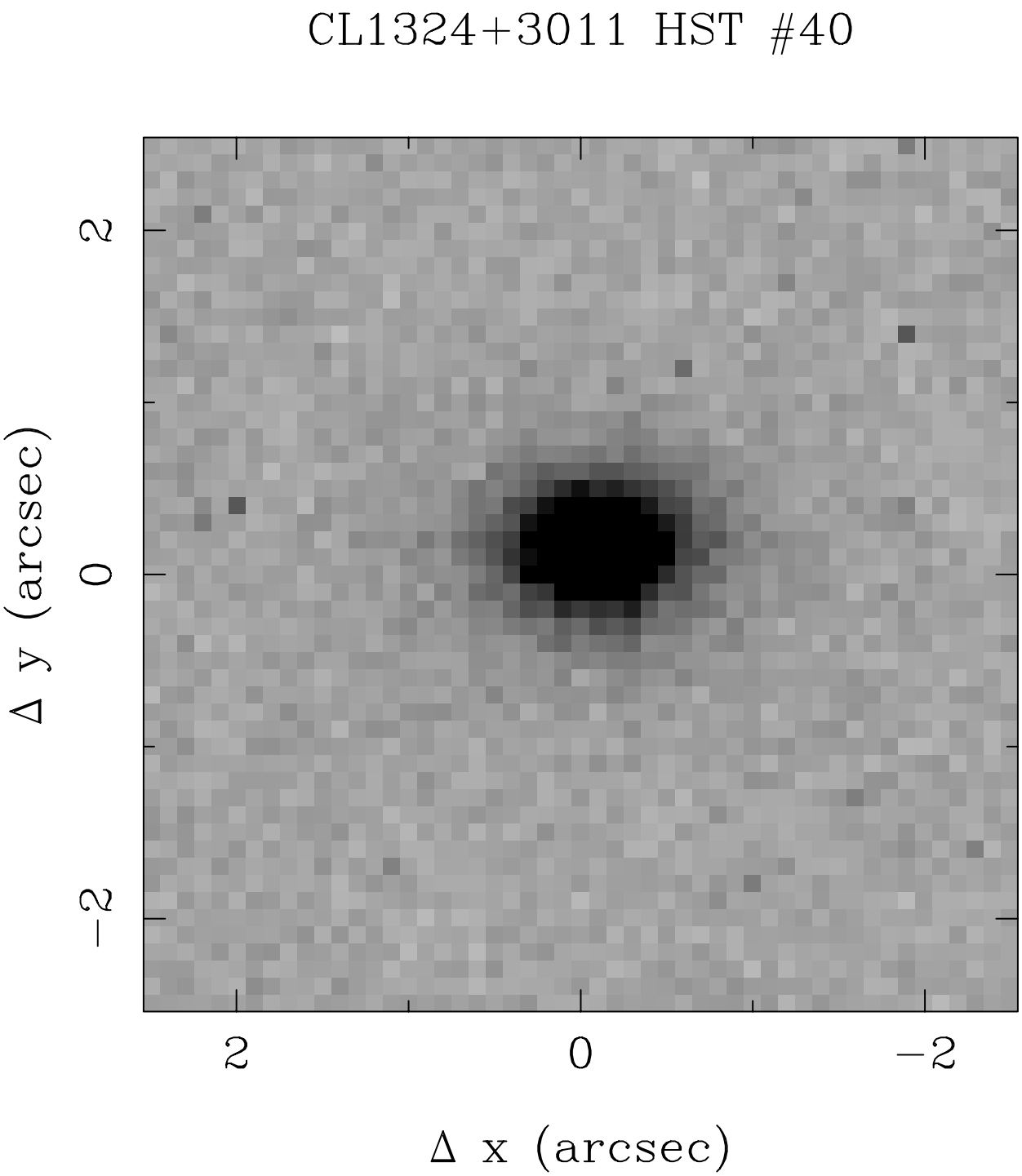

Fig. 1.— HST image of the galaxy HST #40 in Cl 1324 + 3011 ($z = 0.76$) in the $F814W$ bandpass. The half-light radius is $\sqrt{ab} = 0\farcs26$. The box size is $5'' \times 5''$.

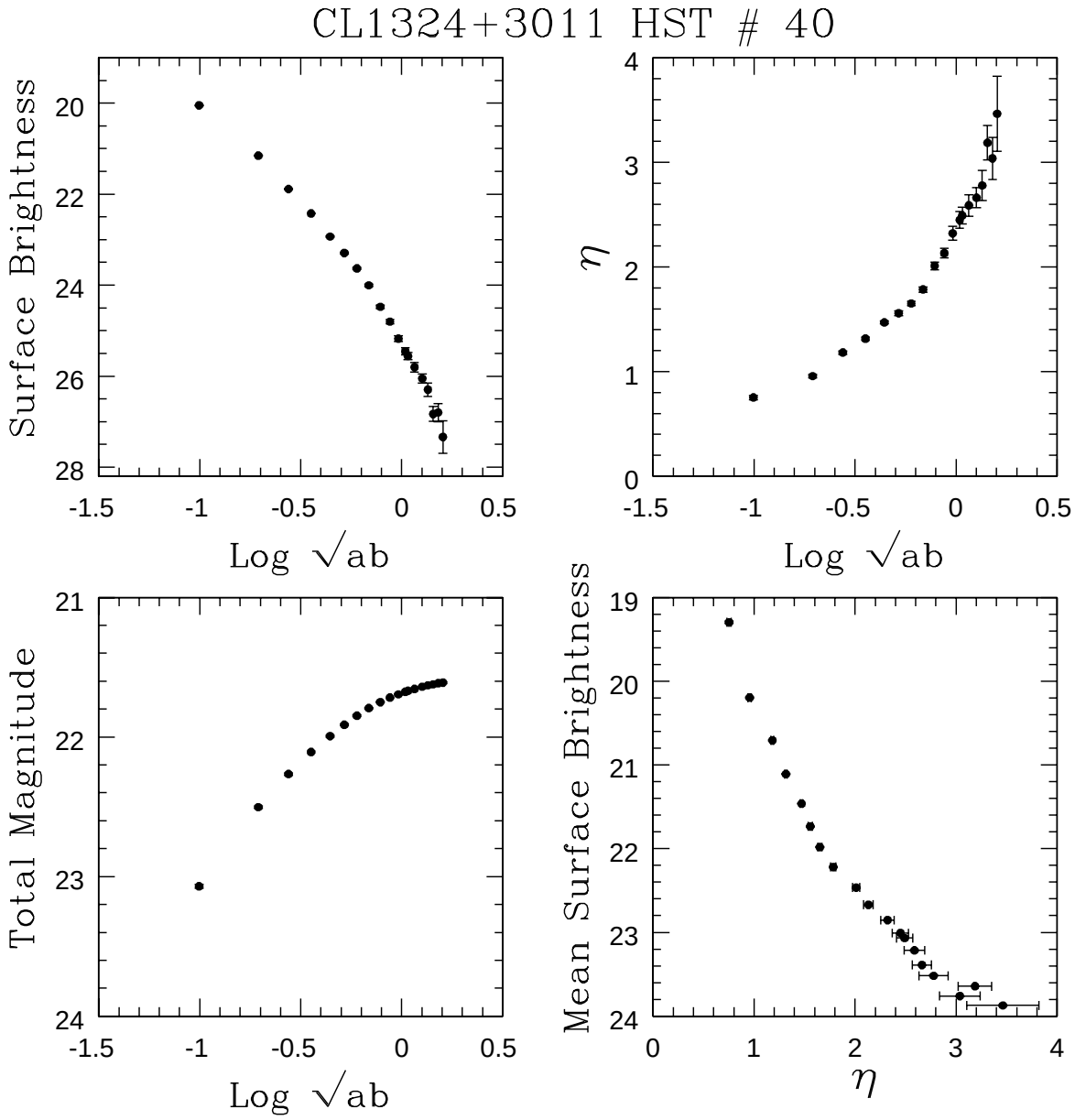

Fig. 2.— The four diagnostic diagrams for galaxy HST #40 in Cl 1324+3011 from the data given in Table 1. The photometry is measured in the $F814W$ bandpass of the HST filter system. The relation between $F814W$ and Cousins I magnitudes is given in equation (2). The units of the surface brightness are magnitudes per square arcseconds, and the units of $\sqrt{ab}$ are in arcseconds.

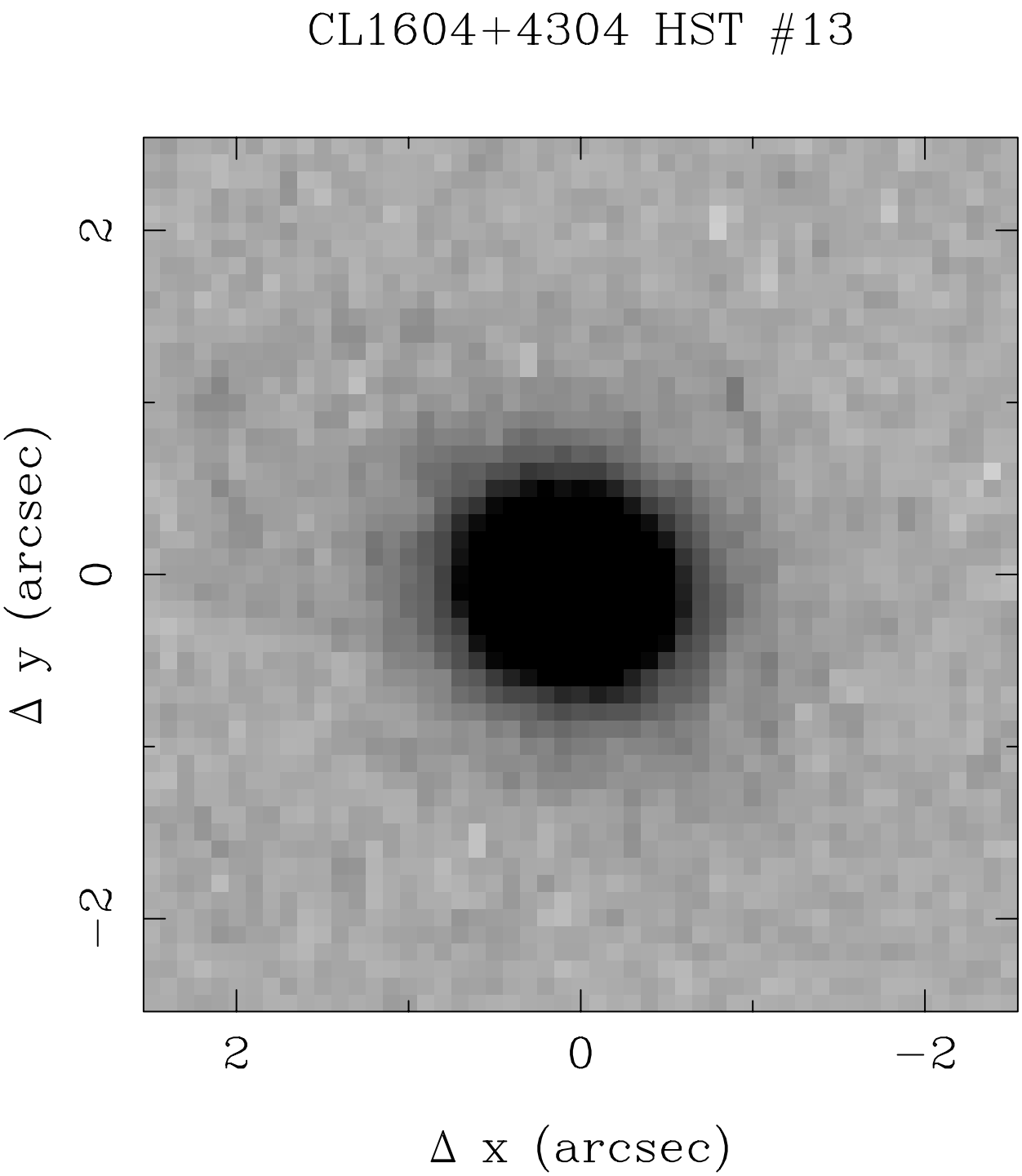

Fig. 3.— HST image of the galaxy HST #13 in Cl 1604+4304 ($z = 0.90$) in the $F814$ bandpass. The half-light radius is $\sqrt{ab} = 0\farcs36$. The box size is $5'' \times 5''$.

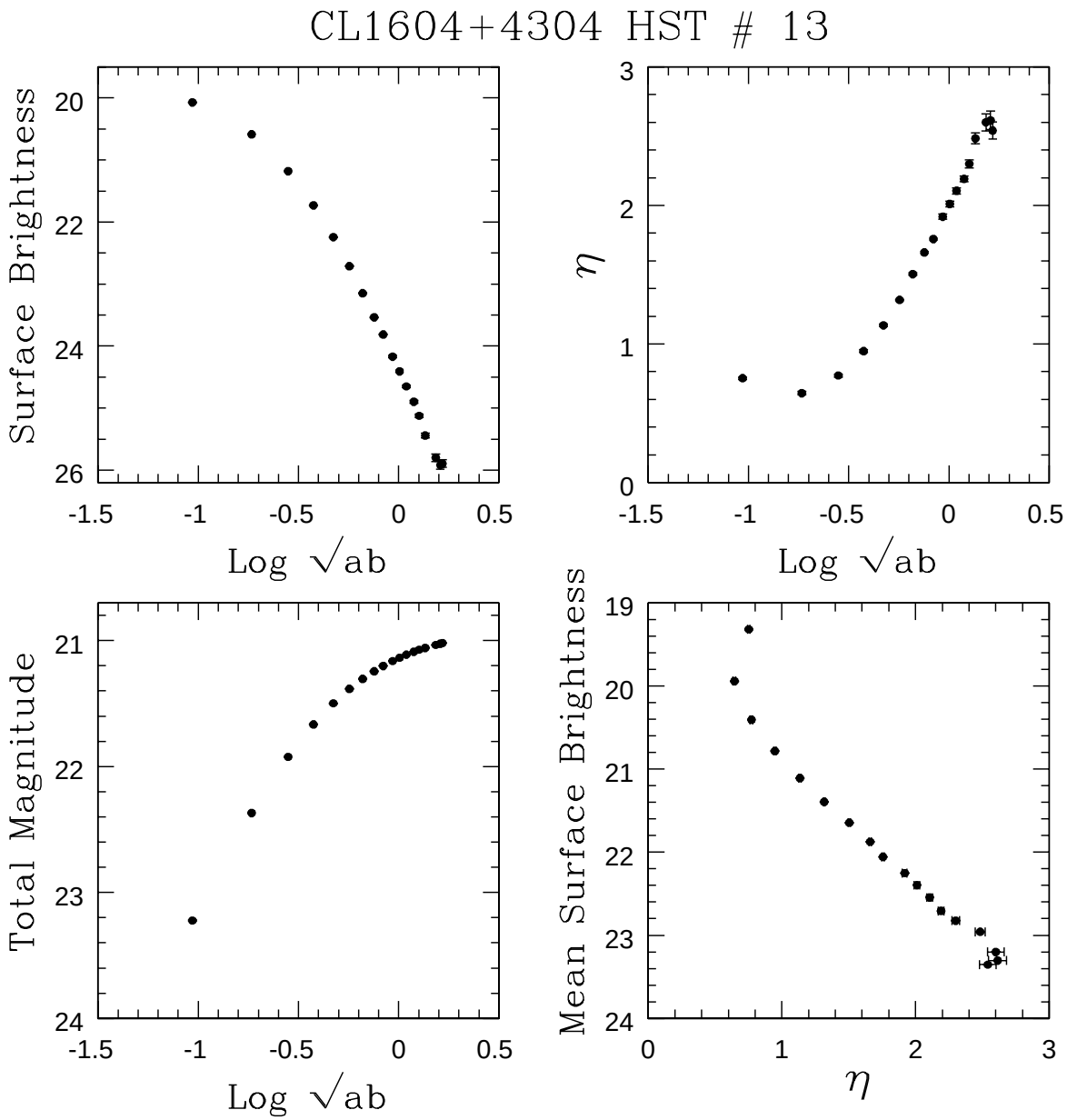

Fig. 4.— Same as Figure 2 but for galaxy HST #13 in Cl 1604+4304. The photometry is given in the $F814W$ filter system.

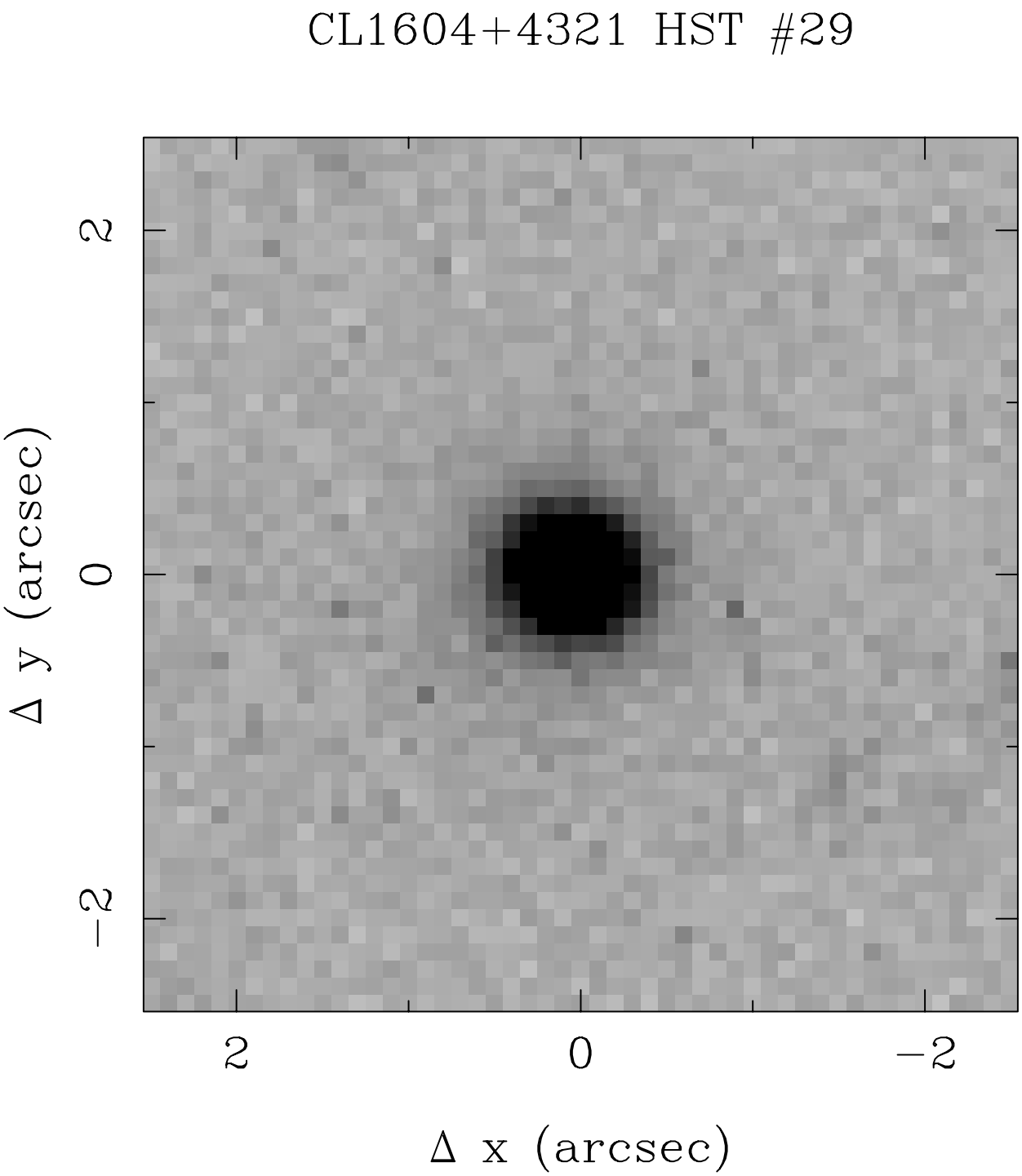

Fig. 5.— HST image of the galaxy HST #29 in Cl 1604+4321 ($z = 0.92$) in the $F702W$ bandpass. The half-light radius is $\sqrt{ab} = 0\farcs35$. The box size is $5'' \times 5''$.

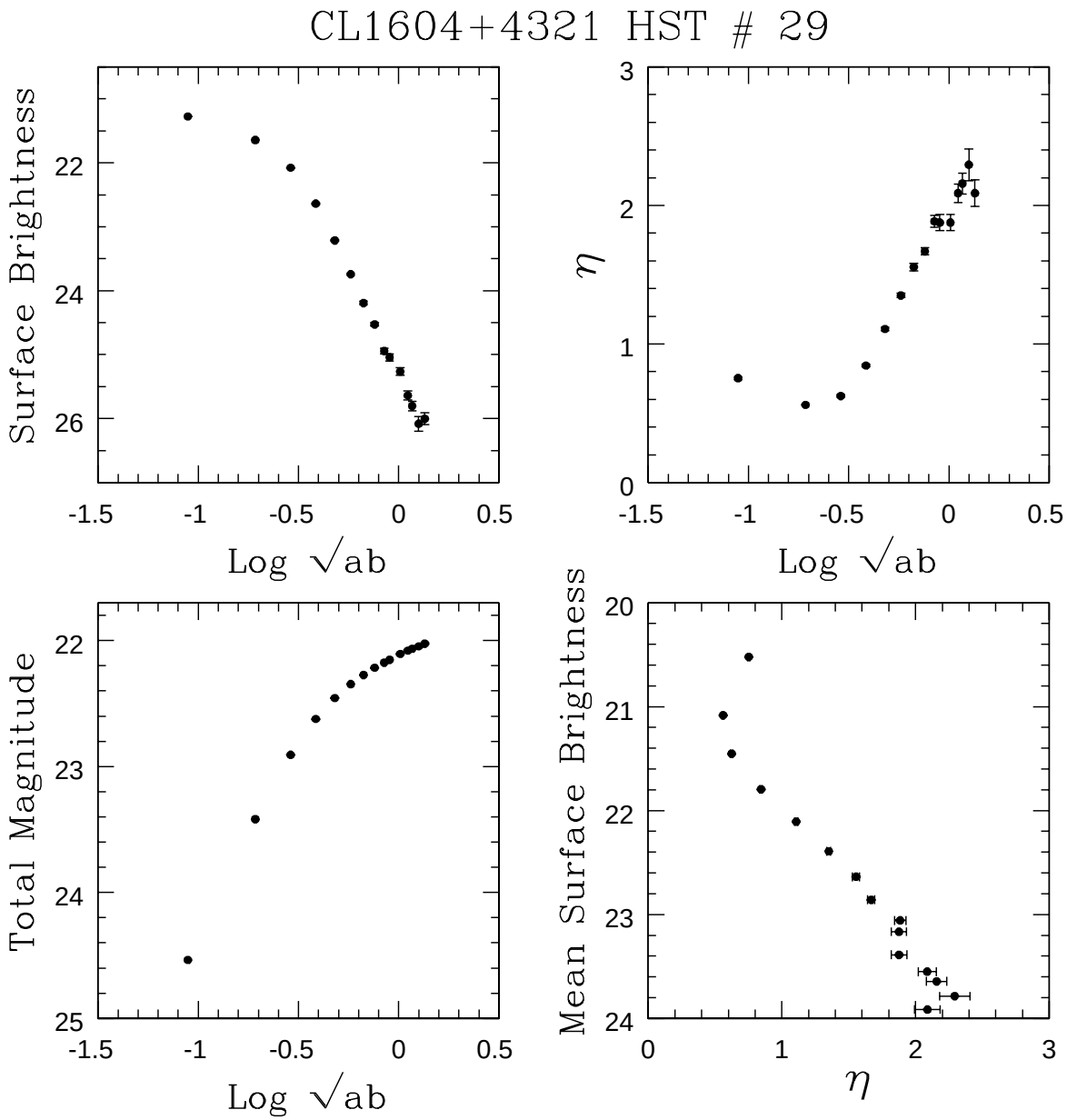

Fig. 6.— The same as Figures 2 & 4 but for galaxy HST #29 in Cl 1604+4321. The photometry is measured in the HST $F702W$ photometric system.

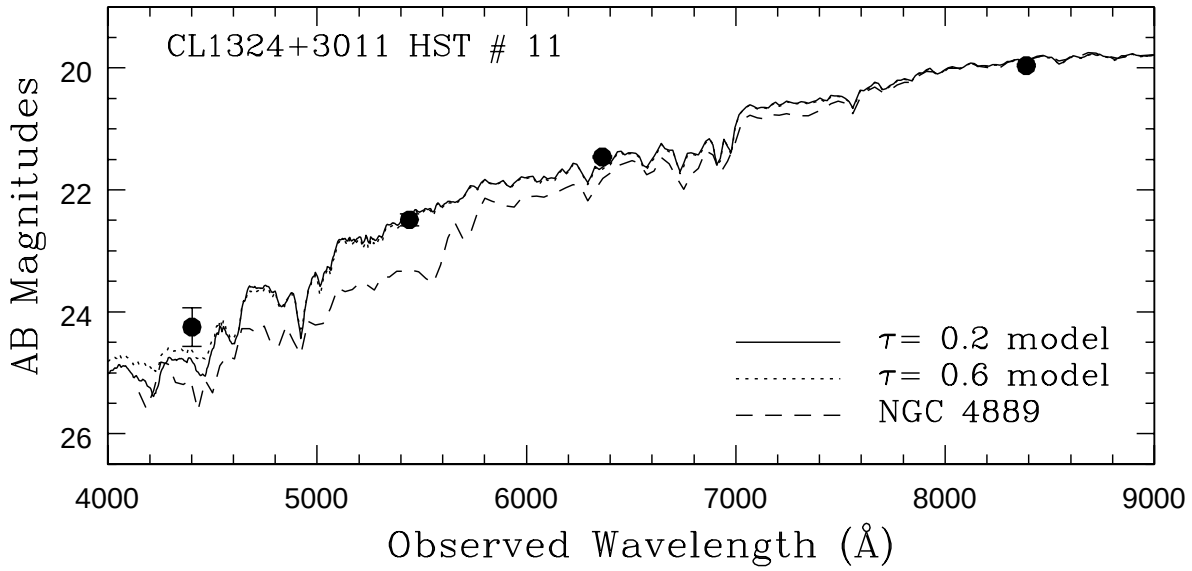

Fig. 7.— The best-fit Bruzual & Charlot (1993) models to the observed broad-band ($BVRI$) AB magnitudes (shown by the closed circles) of galaxy HST #11 in Cl 1324+3011. The best-fit models have been redshifted to the appropriate observed wavelength by $(1+z)$, where $z = 0.7580$ for HST # 11 (PLO01). The $\tau = 0.2$ Gyr model (solid line) and the $\tau = 0.6$ Gyr model (dotted line) are shown. The final best-fit spectrum is nearly identical in both cases (see §3). For comparison, we also show the spectrum for a nearby elliptical galaxy, NGC 4889 (dashed line), redshifted to $z = 0.7580$ and normalized to the I band magnitude of HST #11. This spectrum would represent the no-evolution case, which is clearly inconsistent with the observed data.